


RESEARCH

Open Access



A novel lncRNA FLJ promotes castration resistance in prostate cancer through AR mediated autophagy

Yingying Wu^{1,2†}, Shaojie Cheng^{3†}, Ting Zhang², Leilei Wang², Ting Li², Yongbo Zheng⁴, Guo Yang⁴, Xiaohou Wu⁴, Chunli Luo², Tingmei Chen² and Liping Ou^{2*} 

Abstract

Background Progression to castration resistance is the leading cause of death in prostate cancer patients. Long non-coding RNAs (lncRNAs) have recently become a focal point in the regulation of cancer development. However, few lncRNAs associated with castration-resistant prostate cancer (CRPC) have been reported.

Methods Firstly, we explore the CRPC associated lncRNAs by RNA sequencing and validated using quantitative polymerase chain reaction (qRT-PCR) and RNA fluorescence in situ hybridization (RNA-FISH). The clinical significance of FLJ was evaluated in a collected cancer cohort. Functional loss assays were performed to assess the effects of FLJ on CRPC cells both in vitro and in vivo. The regulatory mechanism of FLJ was investigated using immunohistochemistry (IHC), qRT-PCR, dual-luciferase reporter assays, and chromatin immunoprecipitation (ChIP) assays.

Results FLJ is highly expressed in CRPC and is associated with higher stages and Gleason scores in prostate cancer. FLJ is strongly positively correlated with androgen receptor (AR), which acts as a transcription factor and directly binds to the FLJ promoter region to enhance its transcription. Knockdown of FLJ inhibits CRPC cell proliferation and increases sensitivity to castration and enzalutamide (ENZA) in vitro. Mechanistically, FLJ promotes castration resistance in prostate cancer cells by inhibiting AR nuclear import and cytoplasmic protein degradation, thereby activating the androgen-independent AR signaling pathway. Importantly, in vivo experiments showed that FLJ knockdown inhibited tumor growth and enhanced the therapeutic effect of ENZA.

Conclusions This study identifies a novel regulatory mechanism by which lncRNA FLJ promotes CRPC progression. Sustained AR activation in CRPC acts as a transcription factor to upregulate FLJ expression. FLJ circumvents the traditional androgen-dependent survival mechanism by inhibiting AR nuclear entry and cytoplasmic protein degradation, thereby activating the AR signaling pathway. Targeting the FLJ-AR signaling axis may represent a novel therapeutic strategy for patients with castration-resistant prostate cancer.

Keywords Castration resistance prostate cancer (CRPC), lncRNA FLJ, Castration resistance, Androgen receptor (AR), Autophagy

[†]Yingying Wu and Shaojie Cheng contributed equally to this work.

*Correspondence:

Liping Ou

ouliping963@cqmu.edu.cn

Full list of author information is available at the end of the article



© The Author(s) 2025. **Open Access** This article is licensed under a Creative Commons Attribution-NonCommercial-NoDerivatives 4.0 International License, which permits any non-commercial use, sharing, distribution and reproduction in any medium or format, as long as you give appropriate credit to the original author(s) and the source, provide a link to the Creative Commons licence, and indicate if you modified the licensed material. You do not have permission under this licence to share adapted material derived from this article or parts of it. The images or other third party material in this article are included in the article's Creative Commons licence, unless indicated otherwise in a credit line to the material. If material is not included in the article's Creative Commons licence and your intended use is not permitted by statutory regulation or exceeds the permitted use, you will need to obtain permission directly from the copyright holder. To view a copy of this licence, visit <http://creativecommons.org/licenses/by-nc-nd/4.0/>.

Introduction

Prostate cancer (PCa) is the second most common cancer among men worldwide and the fifth leading cause of cancer death [1]. Statistics indicate that 13 out of every 100 men are diagnosed with PCa during their lifetime [2]. The development and progression of PCa are closely related to androgens. Endocrine therapy targeting the inhibition of androgens or androgen receptors (AR), known as androgen deprivation therapy (ADT), is the most effective treatment for early PCa [3–5]. However, the majority of cases become resistant to treatment within 1–2 years, progressing to castration-resistant prostate cancer (CRPC) [6, 7].

The primary mechanism of CRPC is believed to be the sustained activation of AR. Enzalutamide (ENZA) is a first-line treatment for CRPC, but resistance—either congenital or acquired—often develops, leading to tumor recurrence, metastasis, and ultimately patient death. This resistance is closely associated with abnormal reactivation of AR [8, 9]. As CRPC is almost inevitable, there is an urgent need to study the cellular pathways and molecular mechanisms that enable tumors to evade ADT and develop resistance, particularly the abnormal reactivation of AR in CRPC.

Non-coding RNAs, especially long non-coding RNAs (lncRNAs), exhibit high tissue and tumor specificity, playing unique regulatory roles in various cancers and emerging as candidate molecules for novel biomarkers [10]. However, the potential application of lncRNAs in prostate cancer has not been fully explored. Basic research has confirmed the regulatory crosstalk between lncRNAs and AR [11, 12]. Yet, whether lncRNAs are involved in the sustained activation of the AR signaling pathway in CRPC and the progression of ENZA resistance, along with the specific regulatory mechanisms, remains unclear.

Autophagy is a highly conserved physiological catabolic process [13]. Increasing evidence suggests that autophagy plays a crucial role in resistance to targeted therapy in various cancers, and inhibiting autophagy can resensitize resistant cells to treatment [14, 15]. However, due to its dual role, identifying patients who might benefit most from this approach presents challenges and opportunities, complicating the development of novel inhibitors and clinical trial strategies targeting autophagy. Investigating the molecular network regulating autophagy in the tumor microenvironment to select alternative therapeutic targets may offer an effective treatment strategy for advanced cancer.

In this study, we demonstrated that FLJ is highly expressed in CRPC and tissues of CRPC patients. Mechanistically, the sustained activation of AR in CRPC acts as a transcription factor to promote FLJ transcription.

FLJ inhibits AR nuclear entry in the cytoplasm of CRPC, thereby preventing AR protein downregulation and activating the AR signaling pathway. Additionally, targeting FLJ can enhance AR-mediated autophagy-induced castration resistance, inhibit tumor growth *in vivo*, and improve ENZA treatment sensitivity. In summary, our work elucidates the crucial role of FLJ in the progression of CRPC and proposes a new strategy for cancer treatment.

Materials and methods

Clinical samples

Six pathological tissue samples of prostate cancer, along with their matched adjacent tissues, were collected from patients who underwent surgery at the Department of Urology, First Affiliated Hospital of Chongqing Medical University, between 2021 and 2022. Additionally, pathological tissue sections from paraffin blocks were obtained from the Clinical Pathology Diagnostic Center of the same hospital between 2017 and 2022, including 22 cases of benign prostatic hyperplasia and 50 cases of prostate cancer. Clinical and pathological parameters such as age, pathological stage, Gleason score, lymph node metastasis, and distant metastasis were also documented. All tissue samples were diagnosed by pathology experts, and informed consent was obtained from patients and their families, with ethical approval granted by the Ethics Committee of Chongqing Medical University.

Cell culture

Normal human prostate epithelial cells (RWPE-1), hormone-sensitive prostate cancer cells (LncP), castration-resistant prostate cancer cells (22Rv1, C4-2, C4-2B), and AR-negative prostate cancer cells (PC3, DU145) were purchased from the American Type Culture Collection (ATCC). All cells were cultured in Roswell Park Memorial Institute (RPMI)-1640 medium (Gibco, Shanghai, China), supplemented with 10% fetal bovine serum (FBS; Shanghai ExCell Biology, China) and 1% penicillin–streptomycin. Cells were maintained in a humidified atmosphere with 5% CO₂ at 37 °C.

qRT-PCR and RNA sequencing

Total RNA was extracted utilizing the TRIzol reagent (Takara, Japan), and cDNA synthesis was performed with the PrimeScript RT Reagent Kit (Takara, Japan). Quantitative real-time PCR was conducted using the SYBR Premix Ex Taq II kit (Takara, Japan). The primer sequences employed in qRT-PCR are detailed in Supplementary Table 1. RNA sequencing was conducted by SHBIO (Shanghai, China), and the data were analyzed using R software with the DEGseq package. The criteria for

identifying significant differences were set at a $\log_2|\text{fold change}| \geq 1$ and a P -value of < 0.05 .

Bioinformatics analysis

FLJ expression in prostate cancer was analyzed using the TCGA database, which included 489 prostate cancer tissue samples and 51 normal prostate tissue samples. FLJ expression across various cancers was analyzed using the Sangerbox biomedical data analysis platform, including 495 prostate cancer tissue samples and 52 normal prostate tissue samples. The microarray data used in this study were obtained from the Gene Expression Omnibus (GEO) datasets under accession numbers GSE28680.

RNA-fluorescence in situ hybridization (FISH)

The distribution of lncRNA FLJ in BPH and PCa paraffin tissue sections was detected using a lncRNA FISH Probe Mix and Fluorescence in situ Hybridization Kit (RIBO Bio, China). FISH was conducted according to the manufacturer's instructions. In brief, the sections were fixed with 4% polyformaldehyde for 15 min and then permeabilized using 0.5% Triton X-100 for 30 min. Afterward, the sections were incubated overnight at 4 °C with the lncFLJ FISH Probe or a control probe, followed by the application of Cy3-labeled anti-rabbit IgG as the secondary antibody. The images were captured using a confocal microscope.

Plasmid construction and transfection

shRNAs specifically targeting lnc FLJ, AR, and control hairpins were cloned into the PGL3 vector, and cells were transfected with lentiviral constructs expressing either shRNA or shNC for 24 h. Transfected cells were selected with puromycin over a 2-week period to establish stable lines. The sequences of the effective shRNAs are listed in Table S2, Supporting Information. Cells transfected with lentiviral vectors for AR overexpression or with control vectors were similarly selected with puromycin for 2 weeks following a 24-h transfection period. All lentiviruses were obtained from GENE CREATE (Wuhan, China).

Dual-luciferase reporter assay and chromatin immunoprecipitation (ChIP) assay

In summary, HEK293T cells were seeded in a 96-well plate and co-transfected with either the lncFLJ promoter vectors and pcDNA3.1 (+)-AR or a control vector. The pGL3-lncFLJ WT reporter or pGL3-lncFLJ MUT reporter was introduced into HEK293T cells using Lipofectamine 2000, with the Renilla luciferase reporter vector (PRL-TK vector) serving as a control. After 24 h of transfection, cell lysates were harvested, and the activities of Renilla and Firefly luciferase were measured

using a dual-luciferase reporter assay system (Promega, USA). Chromatin immunoprecipitation (ChIP) assays were conducted using the ChIP Kit from Cell Signaling Technology (New York, USA) with AR and control IgG antibodies. The primer sequences for ChIP are listed in Supplementary Table 3.

Immunohistochemical (IHC) analysis

Paraffin-embedded tissue sections were dewaxed using xylene and then rehydrated through a graded series of alcohols. Endogenous peroxidase activity was inhibited with 3% H₂O₂, followed by microwave heating for antigen retrieval. To prevent nonspecific binding, sections were blocked with 5% BSA at 37 °C for 1 h. The sections were then incubated overnight at 4 °C with primary antibodies specific for Ki67, AR, or LC3B (1:1000 dilution, ABclonal, China). Afterward, the sections were treated with the appropriate secondary antibodies at 37 °C for 1 h, followed by staining with diaminobenzidine and counterstaining with hematoxylin. Images were captured using a light microscope.

Western blot (WB) assay

Cell proteins were extracted and subjected to separation using 10% SDS-PAGE gels, followed by transfer onto 0.22 µm PVDF membranes (Millipore, USA). These membranes were then blocked with 5% skim milk powder and incubated overnight at 4 °C with specific primary antibodies. Subsequently, the membranes were treated with the corresponding secondary antibodies, and protein bands were visualized using an ECL detection system (Bio-Rad, USA). β -Actin served as the loading control. The primary antibodies utilized in this study included the following: BAX (Abmart, 1:500), Caspase-3 (Abmart, 1:500), BCL-2 (Abmart, 1:1000), ATG5 (Abmart, 1:1000), Beclin-1 (Abmart, 1:500), P62 (Abmart, 1:500), PI3K (CST, 1:500), P-PI3K (CST, 1:1000), AKT (CST, 1:500), P-AKT (CST, 1:500), mTOR (Abcam, 1:1000), P-mTOR (Abcam, 1:500), ATG4B (Abcam, 1:500), ATG4D (Abcam, 1:500), ULK1 (Abcam, 1:1000), ULK2 (Abcam, 1:1000), AR (ABclonal, 1:1000), KLK3 (Abcam, 1:1000), FABP5 (Abcam, 1:1000).

IC50 assay

Cells (5×10^4 /well) were seeded into a 96-well plate. After cell adhesion, 10 µL of various concentrations of ENZA (MCE, USA) were added to each well. The cells were cultured for 48 h, then washed twice with PBS. The culture medium was replaced, and 10 µL of CCK8 solution (Biosharp, China) was added to each well. The cells were incubated for an additional 2 h. Absorbance was then measured at 450 nm using an enzyme-linked immunosorbent assay (ELISA) reader.

Colony formation assay

Transfected cells were counted and then seeded at a density of 500 cells per 6 cm plate. After 1–2 weeks, the resulting cell colonies were washed with PBS, fixed in ethanol for 10 min, and stained with crystal violet for 20 min. The colonies were subsequently imaged and counted.

Tumor xenograft model

22Rv1 cells (2.5×10^7 cells) with or without lncFLJ knockdown were suspended in 200 μ l PBS and injected subcutaneously into the flanks of 4–6-week-old nude male mice. After 30 days, the mice were sacrificed, and the tumors' maximum (L) and minimum (W) lengths and weights were measured. Tumor volume was calculated using the formula $\frac{1}{2} LW^2$. Hematoxylin and eosin (H&E) staining was conducted to evaluate tissue morphology. The animal experiments were approved by the Animal Care and Use Committee of Chongqing Medical University.

Statistical analysis

Each experiment was conducted in triplicate, with data presented as the mean \pm S.D. derived from three independent trials and analyzed using GraphPad Prism software (version 8.0). For the comparison of two groups, Student's t-test or chi-square test was applied. Pearson's correlation coefficient was used to assess the relationship between lncFLJ and AR expression levels. Statistical significance was determined at $P < 0.05$.

Results

The novel lncRNA FLJ is highly expressed in CRPC and correlated with a poor prognosis in prostate cancer

To explore the effect of lncRNA on the malignancy of CRPC tumors, HSPC cells (LncAP) and CRPC cells (22Rv1) were selected for RNA-Seq screening to identify differentially expressed lncRNAs. The results showed

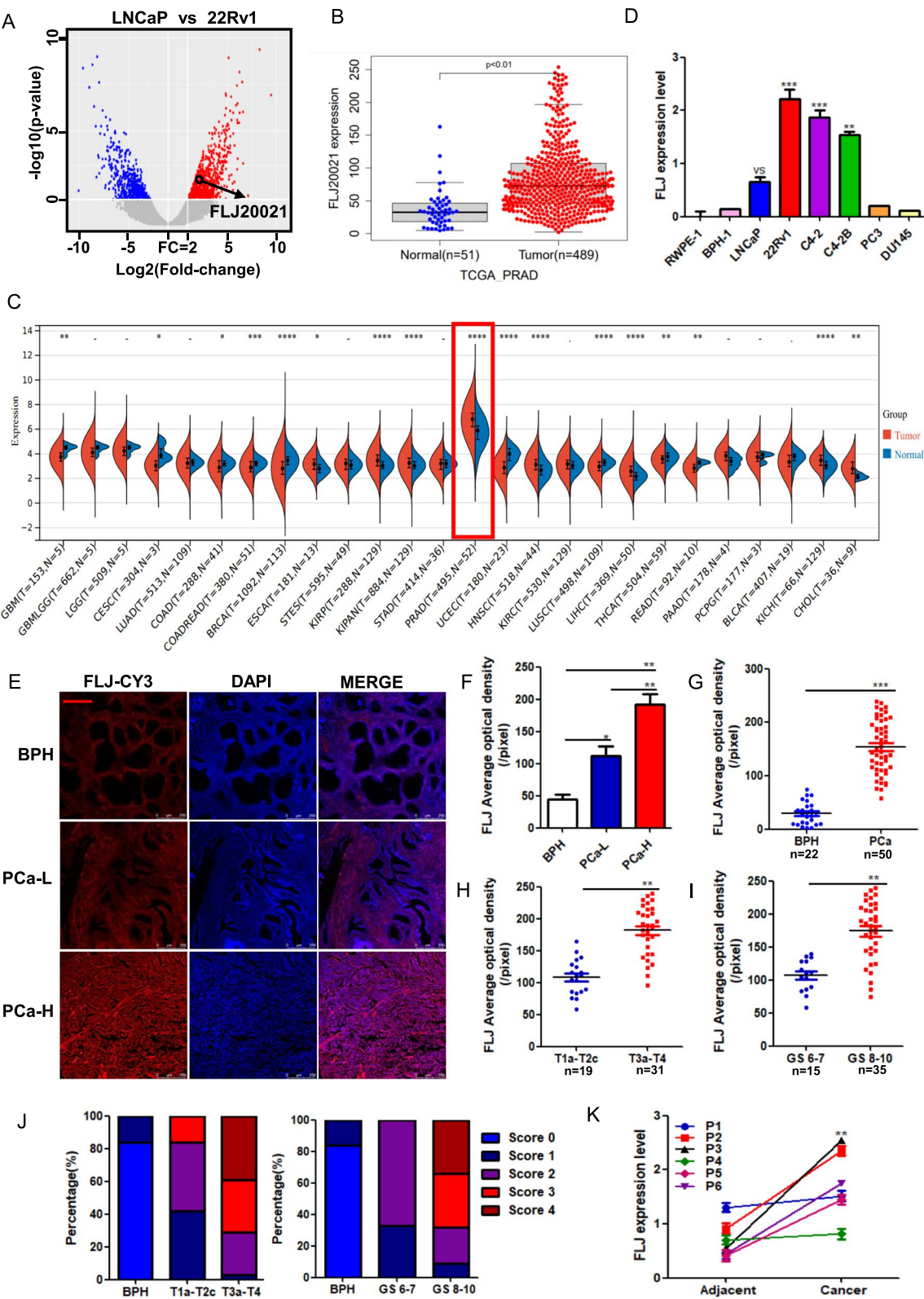
that 1086 transcripts were upregulated and 1460 transcripts were downregulated in CRPC ($|\log_2FC| > 1$, $P < 0.01$). After excluding transcripts with uneven expression levels, lncRNA-FLJ20021 was identified as the most significantly upregulated target in CRPC (Fig. 1A). This novel transcript, named FLJ, had not been previously explored. Similarly, analysis of the GEO dataset revealed that drug-responsive patients (responders) exhibited low levels of FLJ expression, whereas castration-resistant patients displayed the opposite expression pattern (Figure S1A). 489 PCa tissue samples and 51 normal prostate tissue samples from the TCGA database were analyzed. The results showed that FLJ was highly expressed in PCa (Fig. 1B). Next, FLJ expression in various cancer tissues was analyzed using Sangerbox, revealing that FLJ's high expression in PCa is tissue-specific (Fig. 1C), indicating its potential as a molecular diagnostic or therapeutic target in PCa.

Furthermore, FLJ expression in PCa series cells was validated through qRT-PCR, and the upregulated lncRNA FLJ was further confirmed in the CRPC cell line 22Rv1 (Fig. 1D). Interestingly, it was found that FLJ was almost not expressed in AR-negative PCa cells PC3 and DU145, suggesting an association between FLJ and AR (Fig. 1D).

To further determine the clinical significance of FLJ in prostate cancer, FLJ expression was detected by RNA-FISH in a cohort of 22 BPH and 50 PCa paraffin-embedded tissue sections (Fig. 1E), and the average optical density of FLJ fluorescence images was quantified using ImageJ (Fig. 1F). The results showed that, compared with BPH, FLJ was highly expressed in both PCa-L and PCa-H groups, with higher expression in PCa-H than in PCa-L. Overall, FLJ expression in PCa was higher than in BPH (Fig. 1G). To account for tissue heterogeneity, RNA from 6 PCa matched adjacent non-cancerous tissue samples was also collected, confirming high FLJ expression in PCa tissue (Fig. 1K). To investigate whether FLJ is involved in the progression of clinical PCa, the quantitative

(See figure on next page.)

Fig. 1 The FLJ exhibits elevated expression levels in CRPC and is associated with a poor prognosis in prostate cancer. **A** The microarray volcano plot indicates the most significantly upregulated lncRNAs in 22Rv1. lncRNA-FLJ20021 (FLJ) is markedly upregulated in 22Rv1 (right panel). The red dots denote significantly upregulated lncRNAs in 22Rv1, whereas the blue dots represent significantly downregulated lncRNAs in LNCaP. Threshold: $|\log_2FC| > 2$, in comparison to LNCaP, $P < 0.05$. **B** The TCGA database reveals the expression levels of FLJ in 51 normal prostate tissue samples and 489 PCa tissue samples. **C** Sangerbox biomedical data analysis reveals FLJ expression across various cancers, encompassing 52 normal prostate tissue samples and 495 PCa tissue samples. **D** qRT-PCR compared FLJ expression in normal prostate epithelial cells (RWPE-1), benign prostatic hyperplasia cells (BPH-1), androgen-dependent (LNCaP) and androgen-independent (22Rv1, C4-2, C4-2B) PCa cell lines, as well as AR-negative (PC3, DU145) PCa cell lines. **E** Representative RNA-FISH images of FLJ in 22 BPH and 50 PCa paraffin-embedded tissue samples, with a scale bar of 250 μ m. **F** The mean fluorescence intensity of the representative RNA-FISH images was quantified using ImageJ. **G** RNA-FISH results in 22 BPH and 50 PCa paraffin-embedded tissue samples were quantified using ImageJ. **H** RNA-FISH results in 19 PCa paraffin-embedded tissue samples with pathological stages T1a-T2c and 31 samples with stages T3a-T4 were quantified using ImageJ. **I** RNA-FISH results in 15 PCa paraffin-embedded tissue samples with Gleason scores of 6–7 and 35 samples with scores of 8–10 were quantified using ImageJ. **J** Fluorescence images were scored based on mean fluorescence intensity (0–4 points) using ImageJ, and the proportion of scores was analyzed according to pathological stage (left) and Gleason score (right). **K** FLJ expression in 6 PCa tissues and their matched adjacent non-cancerous tissues was analyzed using qRT-PCR



RNA-FISH results were reclassified. The results showed that FLJ expression was higher in 31 tissues at pathological stages 3a-4 compared to 19 tissues at stages 1a-2c (Fig. 1H). Similarly, FLJ expression was higher in 35 tissues with Gleason scores of 8–10 compared to 15 tissues with scores of 6–7 (Fig. 1I). Additionally, higher average fluorescence intensity scores were observed in groups with higher pathological stages and Gleason scores (Fig. 1J). Furthermore, our analysis of TCGA data revealed that FLJ expression levels were elevated in prostate cancer patients with higher pathological stages and Gleason scores (Figure S1B-S1C). Finally, clinical pathological analysis (Table 1) showed that FLJ was associated with pathological staging ($P=0.003$) and Gleason score ($P=0.043$) in PCa patients, but not with age ($P=0.666$),

Table 1 Correlation between FLJ expression and clinicopathological features in PCa patients

Characretistics	Cases (%)	FLJ expression		
		Low	High	P-value
Total patients(N)	50	8	42	
Age (years)				
< 60	11(22)	1(2)	10(20)	0.666
≥ 60	39(78)	7(14)	32(64)	
Histological stage				
T1a–T2c	19(40)	7(16)	12(24)	0.003**
T3a–T4	31(60)	1(0)	30(60)	
Gleason score				
6–7	15(30)	5(10)	10(20)	0.043*
8–10	35(70)	3(6)	32(64)	
Lymphnodes status N				
Negative	27	5(10)	22(44)	0.711
Positive	23	3(6)	20(40)	
Distant metastasis M				
M0	22	2	20	0.439
M1	28	6	22	

* $P<0.05$, ** $P<0.01$

lymph node metastasis ($P=0.711$), or distant metastasis ($P=0.439$). These data indicate that lncFLJ is highly expressed in CRPC and closely associated with prostate malignancies.

LncFLJ is upregulated by AR

Previous research suggested that FLJ may be associated with AR. Considering the important role of AR in PCa, further exploration was conducted to investigate the correlation between FLJ and AR in PCa tissue and CRPC cells. In the same batch of BPH and PCa paraffin-embedded tissue sections, the expression of AR was detected by IHC, and the specimen type was verified by HE staining results (Fig. 2A). The IHC scores were quantified and grouped by pathological stage, revealing that the distribution of AR was consistent with that of FLJ (Fig. 2B). Spearman correlation coefficient analysis indicated a strong positive correlation between FLJ and AR, with a correlation coefficient of $r=0.71$ (Fig. 2C). Correspondingly, the FLJ level was positively correlated with AR in TCGA database (Fig. S1D). The expression of FLJ was shown to increase in a dose-dependent manner (Fig. 2D) and a time-dependent manner (Fig. 2E) following the addition of AR activator DHT. ARN-509, an inhibitor that competes with androgens to bind AR and inhibits AR nuclear translocation to target gene promoter regions, was also tested. The addition of ARN-509 resulted in a dose-dependent (Fig. 2F) and time-dependent (Fig. 2G) decrease in FLJ expression. Following 48 h of DHT treatment and subsequent addition of ARN-509, FLJ expression was reversed (Fig. 2H), indicating that FLJ expression in CRPC cells is regulated by AR.

In PCa, AR acts as a transcription factor to activate downstream signaling pathways that promote tumor cell survival. Further investigation was conducted to determine whether the high expression of AR in CRPC is responsible for the upregulation of FLJ. The JASPAR database predicted two AR transcription factor binding sites, ARE1 and ARE2, in the FLJ promoter region, each with scores greater than 5 (Fig. 2I). Based on these sequences,

(See figure on next page.)

Fig. 2 FLJ expression is positively correlated with AR and AR directly regulates FLJ transcription. **A** Representative images of HE staining (top) and IHC detection of AR (bottom) in paraffin-embedded tissue sections from 22 cases of BPH and 50 cases of PCa, with a scale bar of 200 μm. **B** Quantification of AR staining in paraffin-embedded tissue sections from 22 cases of BPH, 19 cases of PCa with pathological stages T1a-T2c, and 31 cases of PCa with stages T3a-T4, based on AR staining scores. **C** The correlation between FLJ fluorescence scores and AR staining scores in 50 paraffin-embedded PCa tissue sections was analyzed using Spearman correlation. **D, E** qRT-PCR analysis of FLJ expression in response to dose- and time-dependent changes induced by the AR agonist DHT. **F, G** qRT-PCR analysis of FLJ expression in response to dose- and time-dependent changes induced by the AR inhibitor ARN-509. **H** qRT-PCR analysis of FLJ expression following 48 h of treatment with DHT and ARN-509. **I** Schematic representation of AR binding sites ARE1 and ARE2 within the FLJ promoter region. **J** Dual-luciferase assay to assess the activity of FLJ luciferase reporters in wild-type and mutant ARE1 and ARE2 plasmids. **K** Dual-luciferase assay to evaluate the effect of DHT or ARN-509 on FLJ luciferase reporter activity in wild-type and mutant ARE1 plasmids. **L** ChIP assay to assess the impact of DHT or ARN-509 on AR binding to the FLJ promoter region. **M, N** qRT-PCR analysis of FLJ and AR expression following transfection with AR knockdown and overexpression plasmids

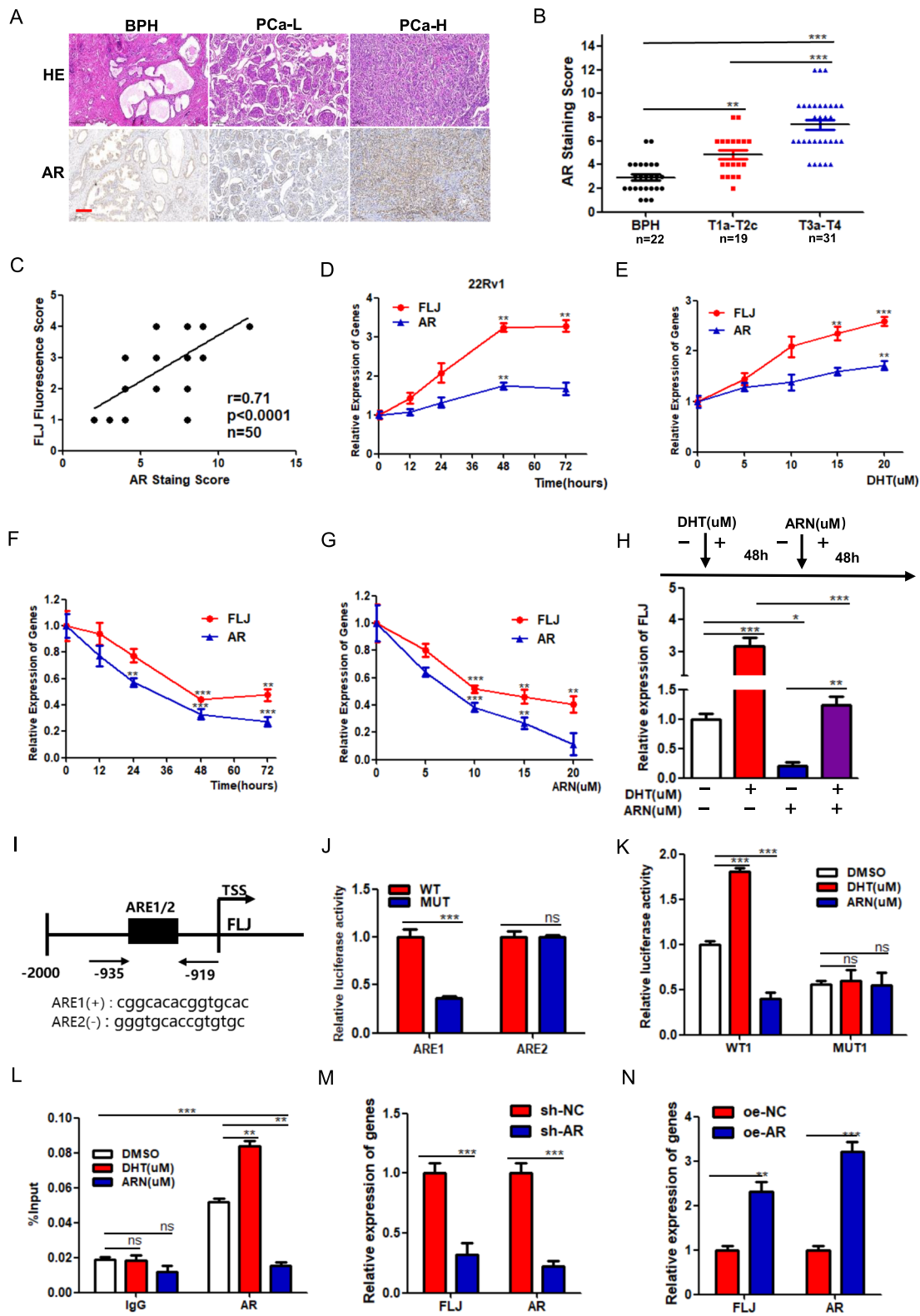


Fig. 2 (See legend on previous page.)

mutant plasmids were designed. Dual luciferase reporter assays showed that, compared with the wild-type control, the luciferase activity of MUT1 decreased, while MUT2 had no effect (Fig. 2J), indicating that the AR transcription factor primarily binds to the ARE1 site in the FLJ promoter region. Further experiments revealed that the luciferase activity of WT1 increased after the addition of DHT and decreased after the addition of ARN, while MUT1 was unaffected by either DHT or ARN (Fig. 2K). This demonstrated the reliability of AR binding to the ARE1 site in the FLJ promoter region. ChIP experiments confirmed that AR antibody precipitation enriched the ARE1 site sequence in the FLJ promoter region, with enrichment levels increasing or decreasing in response to DHT or ARN treatment (Fig. 2L and M). Further verification by qRT-PCR showed that FLJ transcription levels decreased after transfection with AR knockdown plasmids in CRPC cells (Fig. 2M), while FLJ transcription levels increased after transfection with AR overexpression plasmids (Fig. 2N). These data indicate that AR plays a critical role in regulating lncFLJ expression.

FLJ promotes the proliferation of CRPC cells and inhibits sensitivity to in vitro simulated castration

To explore the biological function of FLJ in CRPC, the expression of FLJ in 22Rv1 cells was stably knocked down using lentivirus (Fig. 3A). The proliferation ability of CRPC cells was then tested, and it was shown by the CCK8 assay that FLJ-deficient inhibited the proliferation of CRPC cells (Fig. 3B, left). Simultaneously, an in vitro simulated castration model was constructed by adding 10% hormone-deprived fetal bovine serum (cs-FBS) to RPMI 1640 medium to deplete androgens. Compared with the control group, knocking down FLJ expression in the cs-FBS group resulted in a greater inhibition of cell proliferation (Fig. 3B, right). The clone formation experiment yielded similar results (Fig. 3C, D). However, control cells did not show statistically significant differences between the control group and the cs-FBS group, indicating that FLJ inhibits the responsiveness of CRPC cells to androgen deprivation, i.e., suppresses in vitro simulated castration sensitivity.

Subsequently, the sensitivity of CRPC cells to the anti-androgen drug ENZA after FLJ knockdown was explored. Compared with the control, the IC₅₀ values of FLJ-low expression cells significantly decreased (Fig. 3E), from 121.4 μ M to 24.61 μ M and 21.19 μ M, respectively (Fig. 3F). Next, the cells were treated with DMSO or 20 μ M ENZA. Compared with the DMSO group, the cell viability of the control cells did not change within 72 h after adding ENZA, while the cell viability of the FLJ-knockdown cells began to decrease after 48 h (Fig. 3G). Furthermore, the control and FLJ-knockdown cells were

treated with 20 μ M and 50 μ M ENZA, respectively. The results showed that the cell viability of the control cells did not change, while the cell viability of the FLJ-knockdown cells significantly decreased (Fig. 3H). These results indicate that knocking down FLJ restored the sensitivity of CRPC cells to ENZA treatment.

FLJ promotes CRPC cell proliferation through trace androgen induced autophagy

The biological function of FLJ in the progression of prostate cancer (PCa) was further explored. It was found that silencing FLJ had no effect on cell cycle distribution (Figure S2A, B) but increased the number of apoptotic cells (Figure S2C, D). Consistently, the expression of apoptosis-associated proteins BAX and Caspase-3 was promoted, while the expression level of BCL-2 was inhibited by FLJ silencing (Figure S2E). Previous research has demonstrated that cell apoptosis is closely related to the progression of cancer resistance and autophagy associated with drug resistance [16]. Therefore, the regulatory effect of FLJ on autophagy in castration-resistant prostate cancer (CRPC) cells was further investigated. Interestingly, the transformation of the autophagy marker protein LC3B from type I to type II was inhibited by FLJ silencing, and the expression of autophagy-related proteins ATG7, ATG5, and Beclin-1 was suppressed, while the expression of P62 was promoted (Figure S2F). Immunofluorescence experiments confirmed that the low expression of FLJ inhibited the number of LC3B fluorescent spots in cells (Fig. 4A, B). These results indicate that autophagy levels in CRPC cells are regulated by FLJ. The effect of FLJ on the classical autophagy regulatory pathway PI3K-AKT-mTOR was then explored. It was found that silencing FLJ did not affect PI3K, AKT, mTOR, or their phosphorylation levels (Figure S2G). Previous studies have proposed an autophagy phenomenon induced by trace amounts of androgens [17, 18]. It was found that, compared to control group cells, trace androgen induction did not significantly upregulate the activity of FLJ-silenced cells, indicating that the responsiveness of CRPC cells to trace androgen induction was inhibited by FLJ silencing. By depriving cells of androgen (cs-FBS) and inducing them with 10 nM DHT, it was found that FLJ silencing inhibited the transformation of LC3B type I to type II and promoted the expression of P62 in both the control and DHT induction groups. After androgen deprivation, there was no significant change in the conversion of LC3B type I to type II or in the expression of P62 (Fig. 4D). Further research found that the number of autophagosomes was inhibited by FLJ silencing in both the control and DHT-induced groups, while the number of autophagosomes after androgen deprivation was not affected by FLJ silencing (Fig. 4E, F). On the other hand,

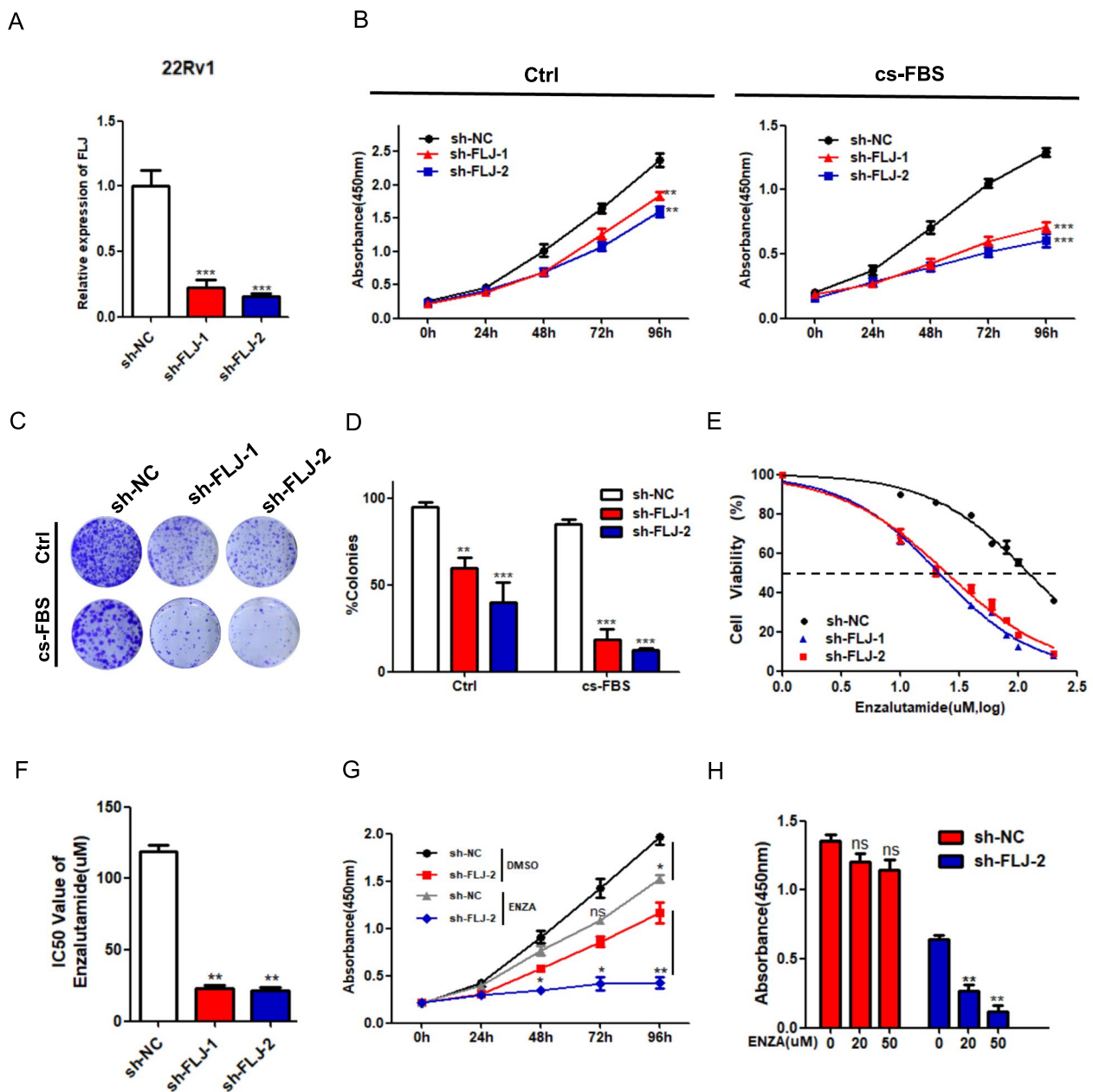


Fig. 3 FLJ enhances CRPC cell proliferation while reducing their sensitivity to castration simulated in vitro. **A** FLJ knockdown efficiency in 22Rv1 cells was measured via qRT-PCR. **B** The impact of FLJ knockdown on cell proliferation and viability under normal and in vitro castration-simulated conditions was assessed through the CCK8 assay. **C** The ability of cells to form colonies following FLJ knockdown was evaluated using a colony formation assay under both normal and castration-simulated conditions in vitro. **D** Quantitative analysis of the colony formation assay results presented in Figure C was performed. **E, F** The IC₅₀ value of ENZA after FLJ knockdown was determined through the IC₅₀ assay. **G** The effect of 20 μM ENZA on cell viability over a period of 0 to 96 h was assessed via the CCK8 assay. **H** Cell viability at 48 h after FLJ knockdown, treated with 20 μM and 50 μM ENZA, was measured using the CCK8 assay

compared with the DMSO group, 10 nM DHT-induced autophagy significantly upregulated the proliferation and colony size of both control and FLJ-silenced cells. After in vitro simulated castration, the control group showed no significant response to cs-FBS after DHT-induced

autophagy compared with the DMSO group, and cell proliferation ability remained upregulated. However, FLJ-silenced cells showed a significant response to cs-FBS, with an upregulation of cell proliferation ability that was not statistically significant (Fig. 4H, I). These

results indicate that FLJ silencing restores the sensitivity of CRPC cells to a simulated castration environment *in vitro* through androgen-induced autophagy.

Finally, the IC₅₀ values of ENZA after DHT-induced autophagy were analyzed. The results showed that after DHT-induced autophagy, the IC₅₀ of FLJ low expression was still downregulated (Fig. 4J, K), indicating that DHT-induced autophagy increased the resistance of CRPC cells to ENZA. However, FLJ knockdown restored the sensitivity of CRPC cells to ENZA, with no significant effect on DHT-induced autophagy. To further validate the function of FLJ in this process, cells were treated with or without DHT induction with a series of gradient times of 20 μ M ENZA. The results showed that after DHT-induced autophagy, the activity of control group cells was upregulated, while there was no difference in the activity of FLJ low-expressing cells (Fig. 4L). Further analysis revealed that in the control group (0 μ M ENZA), both FLJ control cells and FLJ-silenced cells showed upregulation of activity after DHT induction. In the 20 μ M and 50 μ M ENZA treatment groups, the activity of control group cells was upregulated after DHT induction, while there was no difference in the activity of FLJ low-expression cells (Fig. 4M). These results indicate that FLJ silencing restores drug sensitivity of CRPC cells to ENZA through androgen-induced autophagy.

FLJ promotes trace androgen-induced autophagy through AR-mediated pathway

Due to the crucial regulatory role of the androgen receptor (AR) in androgen-induced autophagy [17], further investigation was conducted to determine whether the regulation of androgen-induced autophagy by FLJ is dependent on AR. It was found that silencing FLJ inhibited the conversion of LC3B type I to type II, and the expression of AR protein was also suppressed (Fig. 5A). Subsequently, AR activator DHT (20 μ M) or AR inhibitor ARN-509 (10 μ M) was added to treat the cells. The

results showed that DHT treatment increased the conversion of LC3B type I to type II in both the control and FLJ-silenced cells, while the addition of ARN-509 reduced this conversion. This finding suggests that autophagy is activated with AR activation and inhibited with AR inhibition. However, in FLJ-depleted cells, the conversion of LC3B type I to type II generally showed a decreasing trend (Fig. 5B). Therefore, these results indicate that the modulation of androgen-induced autophagy by FLJ is associated with AR. This conclusion was further confirmed by detecting LC3B fluorescent spots (Fig. 5C, D). Given that androgen-induced autophagy is mediated by the AR-dependent expression of ATG4B, ATG4D, ULK1, and ULK2 [17], the expression levels of these four markers molecules were further explored to determine whether they are regulated by FLJ. Interestingly, compared to FLJ control cells, FLJ silencing inhibited the mRNA and protein expression of these four marker molecules in the DHT-induced group, while no significant differences were observed in the androgen-deprivation group (Fig. 5E, F). These results indicate that the regulation of autophagy by FLJ also depends on androgens.

Finally, AR overexpression plasmids were transfected into FLJ control and FLJ-silenced cells to directly demonstrate the AR-mediated regulation of androgen-induced autophagy by FLJ. Compared to their respective control plasmids, AR overexpression increased the conversion of LC3B type I to type II and the protein expression of the four marker molecules. Furthermore, the inhibition of LC3B type I to type II conversion caused by FLJ silencing was reversed after AR overexpression (Fig. 5G). This result was further validated by detecting the formation of LC3B fluorescent spots (Fig. 5H, I). Additionally, autophagosomes were detected by projection electron microscopy, revealing that AR overexpression increased the number of autophagosomes compared to their respective control plasmids. Moreover, in FLJ-silenced cells, the inhibition of LC3B autophagosome count was

(See figure on next page.)

Fig. 4 FLJ enhances CRPC cell proliferation by inducing autophagy in response to trace levels of androgen. **A** Immunofluorescence was used to detect LC3B expression, an autophagy marker, following FLJ knockdown in cells, with a scale bar of 25 μ m. **B** The mean fluorescence intensity of LC3B in Figure A was quantified. **C** The response of FLJ knockdown to trace androgen stimulation was evaluated using the CCK8 assay. **D** Western blot analysis was conducted to assess the regulation of autophagy markers after FLJ knockdown under conditions of androgen deprivation or the addition of trace androgens. **E** Transmission electron microscopy (TEM) was used to observe autophagosome regulation after FLJ knockdown under androgen deprivation or the addition of trace androgens, with a scale bar of 500 nm. **F** Quantification of autophagosomes in Fig. 4D was performed. **G** The effects of FLJ knockdown on cell proliferation and viability were assessed using the CCK8 assay, following autophagy induction by trace androgens, under normal culture conditions (left) and *in vitro* castration-simulated conditions (right). **H, I** The colony-forming ability after FLJ knockdown was evaluated using a colony formation assay, following autophagy induction by trace androgens, under normal culture conditions (top) and *in vitro* castration-simulated conditions (bottom). **J, K** The IC₅₀ value of ENZA was determined using the IC₅₀ assay after FLJ knockdown and autophagy induction by trace androgens. **L** The effect of 20 μ M ENZA on cell viability over 0–96 h was evaluated using the CCK8 assay after autophagy induction by trace androgens. **M** The impact of FLJ knockdown on cell viability was assessed using the CCK8 assay at 48 h after treatment with 20 μ M and 50 μ M ENZA, following autophagy induction by trace androgens

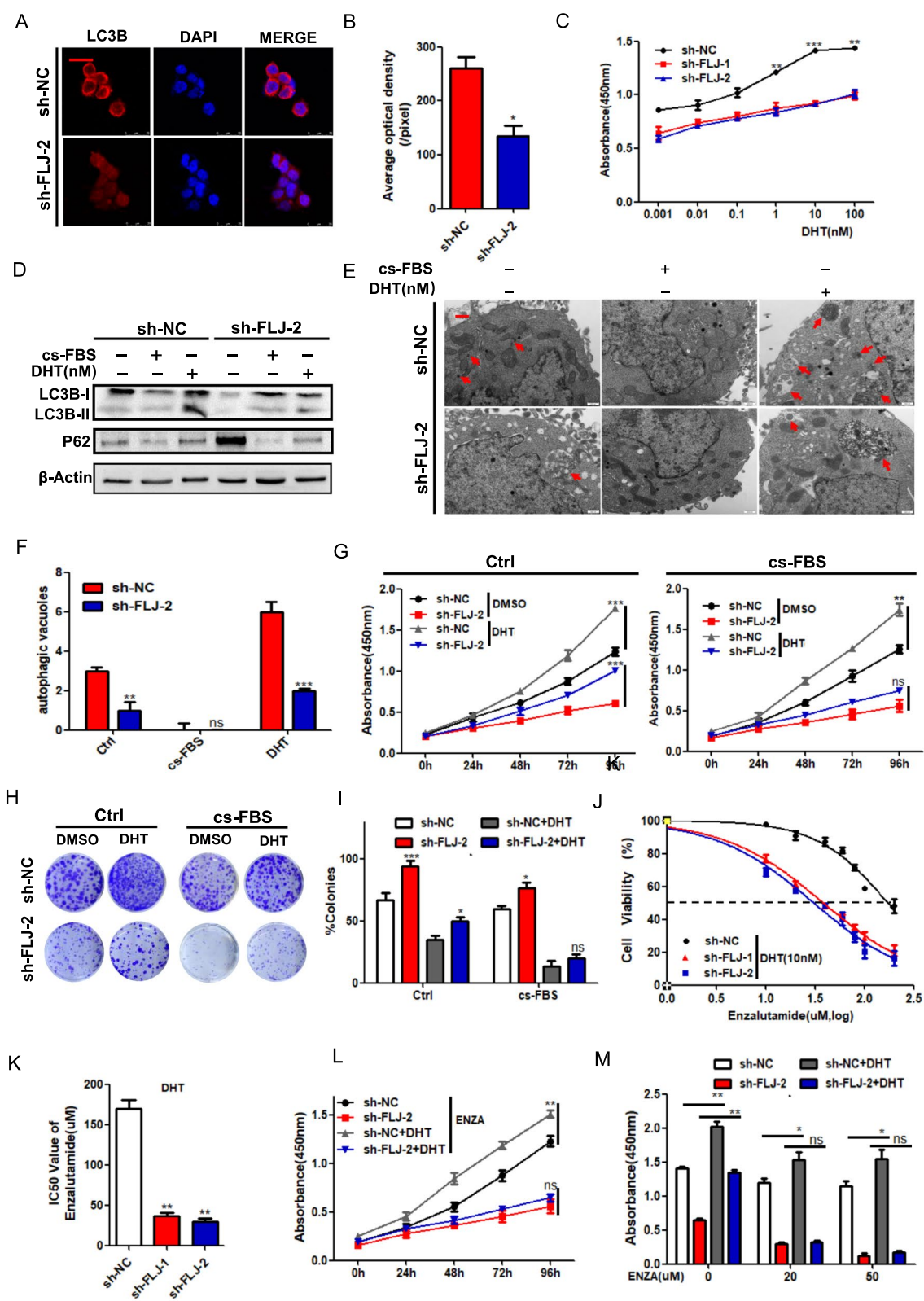


Fig. 4 (See legend on previous page.)

reversed after AR overexpression (Fig. 5I, K). In summary, these results indicate that FLJ regulates androgen-induced autophagy through AR mediation.

FLJ regulates AR localization and stability

The regulatory mechanism of FLJ on AR was subsequently investigated. AR expression levels and those of its target proteins were initially examined in both FLJ control and FLJ-silenced groups. Silencing FLJ significantly reduced the protein expression of AR and its target genes, KLK3 and FABP5 (Fig. 6A). However, FLJ silencing did not significantly affect the mRNA expression of AR or its target genes KLK3 and FABP5 (Fig. 6B), suggesting that FLJ primarily regulates AR at the post-transcriptional level. Using the IncLocator website, FLJ was predicted to be primarily localized in the cytoplasm (Fig. 6C). This prediction was confirmed by RNA-FISH and nuclear-cytoplasmic fractionation experiments, which demonstrated that FLJ is predominantly located in the cytoplasm (Fig. 6D, E). Similarly, it was found that FLJ in C4-2 and C4-2B cells was predominantly localized in the cytoplasm, as confirmed by nuclear-cytoplasmic fractionation (Figure S2H). Immunofluorescence analysis revealed that AR protein expression in the cytoplasm significantly decreased, while its nuclear expression increased, following FLJ silencing (Fig. 6F). Quantitative analysis showed that the overall fluorescence intensity of AR protein decreased after FLJ silencing (Fig. 6G). Furthermore, nuclear-cytoplasmic fractionation revealed that FLJ silencing primarily suppressed AR protein expression in the cytoplasm while increasing it in the nucleus, compared to the FLJ control (Fig. 6H). These findings suggest that FLJ silencing promotes AR nuclear import while inhibiting AR expression in the cytoplasm. Further studies revealed that FLJ silencing significantly accelerated AR protein degradation when cells were exposed to varying time gradients of cycloheximide (CHX), compared to the FLJ control group (Fig. 6I). These results indicate that FLJ regulates cytoplasmic AR protein stability via the proteasome degradation pathway.

Essential role of FLJ in modulating sensitivity to ENZA treatment and tumorigenesis

As previously mentioned, we found that drug responsive patients (responders) exhibited a low expression pattern of FLJ, while castration resistant patients showed the opposite expression pattern (Supplementary Figure S1A). Thus, the tumor-promoting role of FLJ in AR-related tumorigenesis was investigated in vivo. FLJ control cells and FLJ-silenced cells were subcutaneously injected into male nude mice aged 4 to 6 weeks. Two weeks after tumor formation, DMSO or ENZA dissolved in corn oil was administered via oral gavage every 2 days at a dose of 10 mg/kg for 2 weeks (Fig. 7A). In comparison to the control group, FLJ knockdown in CRPC cells significantly reduced tumor volume; after ENZA treatment, the tumor volume in the FLJ-silenced group was further significantly reduced compared to the DMSO group (Fig. 7B). Notably, the body weight of nude mice in the FLJ-silenced group significantly increased following ENZA treatment (Fig. 7C). Moreover, the size and weight of tumors formed in the FLJ knockdown group in CRPC cells were significantly lower than those in the control group. In comparison to the DMSO group, tumor size and weight were further significantly reduced following FLJ knockdown combined with ENZA treatment, leading to maximum inhibition of tumor growth (Fig. 7D, E). These findings indicate that FLJ knockdown inhibited tumor growth in vivo and enhanced the therapeutic efficacy of ENZA. IHC results and quantitative staining scores demonstrated that FLJ silencing inhibited the expression of AR, LC3B, and Ki67 in tumors, while FLJ knockdown combined with ENZA treatment further reduced the expression levels of these molecules (Fig. 7F–I). Interestingly, FLJ expression levels were reduced in the ENZA treatment group compared to the DMSO group, with a more pronounced decrease observed in the FLJ knockdown combined with ENZA treatment group (Fig. 7J). These results suggest that FLJ expression levels were suppressed in vivo following AR

(See figure on next page.)

Fig. 5 FLJ promotes autophagy induced by trace androgens via the AR-mediated pathway. **A** The expression of AR and the autophagy marker LC3B following FLJ knockdown was assessed by WB. **B** The expression of LC3B, an autophagy marker, after AR activation and inhibition was evaluated by WB. **C** The fluorescence intensity of LC3B following AR activation and inhibition was measured using immunofluorescence, with a scale bar of 25 μ m. **D** The mean fluorescence intensity of LC3B in **C** was quantified. **E** The pathway proteins involved in AR-mediated autophagy induced by trace androgens and their dependency on trace androgens after FLJ knockdown were assessed by WB. **F** The pathway molecules involved in AR-mediated autophagy induced by trace androgens and their dependency on trace androgens following FLJ knockdown were evaluated by qRT-PCR. **G** The effect of AR overexpression on LC3B expression and AR-mediated autophagy pathway proteins induced by trace androgens following FLJ knockdown was evaluated by WB. **H** The effect of AR overexpression on LC3B fluorescence intensity after FLJ knockdown was measured using immunofluorescence, with a scale bar of 25 μ m. **I** The effect of AR overexpression on autophagosomes after FLJ knockdown was evaluated using TEM, with a scale bar of 500 nm. **J** Quantification of the average fluorescence intensity of LC3B in Fig. 5H. **K** Quantification of autophagosomes presented in **I**

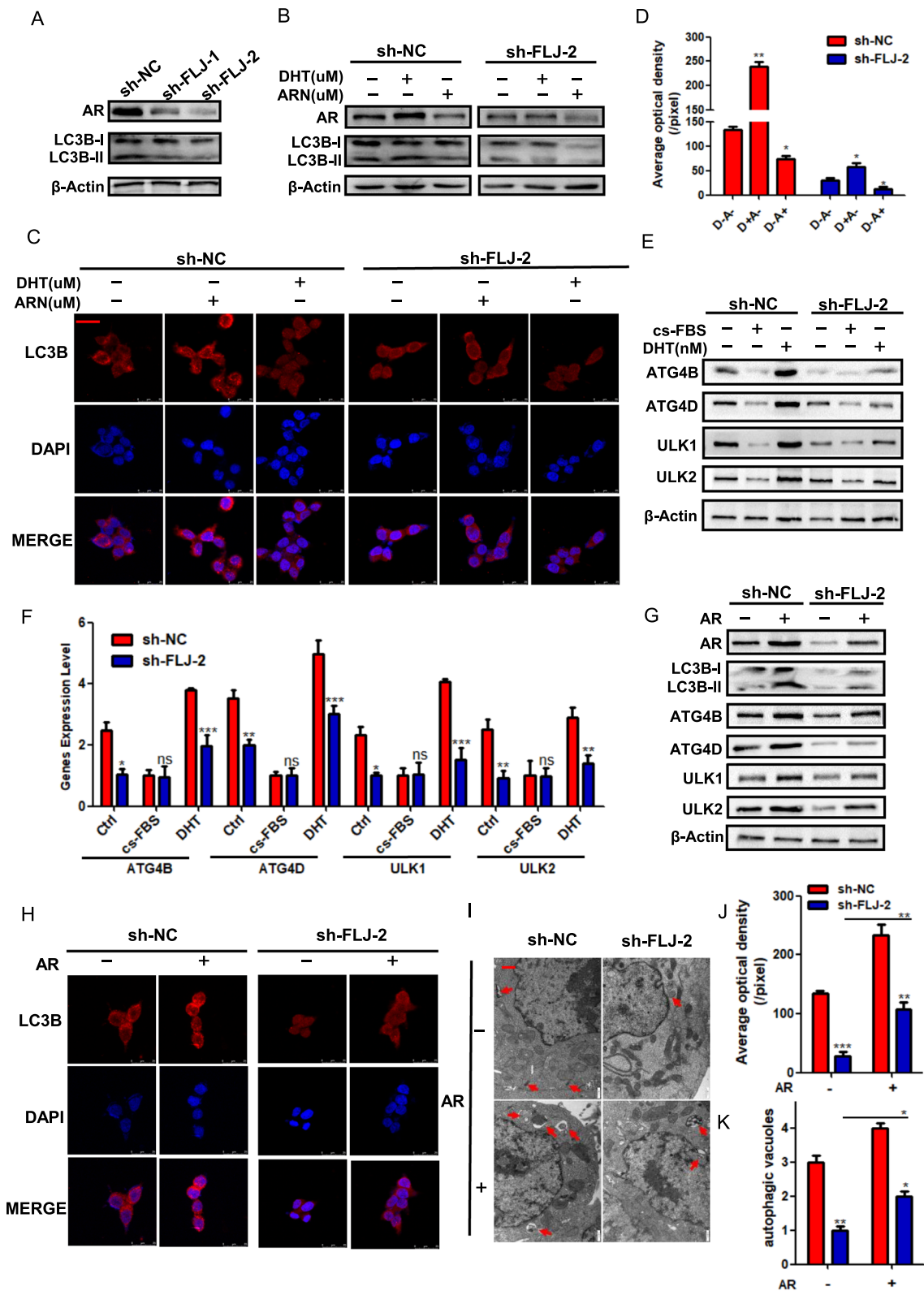


Fig. 5 (See legend on previous page.)

inhibition by ENZA treatment, confirming the role of AR in regulating lncFLJ expression.

Discussion

LncRNAs have been implicated in the progression of castration-resistant prostate cancer (CRPC) [19–21]. For instance, LncRNA HOTAIR enhances androgen receptor-mediated transcriptional programs, driving the development of CRPC [19]. LncRNA PTTG3P facilitates CRPC progression by upregulating PTTG1 [20]. Additionally, LncRNA HOXD-AS1 is overexpressed in CRPC cell lines and promotes CRPC progression by interacting with the WDR5/MLL1 complex [21]. Altered LncRNA expression profiles in CRPC are considered one of the driving forces behind cellular transformation, suggesting that LncRNAs play significant biological roles in prostate cancer progression and could serve as valuable biomarkers for clinical diagnosis and treatment. In this study, we screened for novel targets related to CRPC progression using RNA-Seq and identified a novel AR-related LncRNA named FLJ. FLJ is significantly upregulated in PCa cell lines and patient tissues and is associated with higher pathological stages and Gleason scores in PCa. These findings suggest that FLJ functions as a tumor promoter in PCa progression and may serve as a potential biomarker for PCa progression and prognosis.

Nearly all CRPC cases involve aberrant activation of AR signaling [22]. However, research on AR-regulated LncRNAs remains relatively limited. Known androgen-regulated LncRNAs are generally associated with AR reactivation. For example, androgen-repressed HOTAIR increases AR expression by blocking the E3 ubiquitin ligase MDM2, which targets AR for ubiquitination, thereby promoting the post-translational stabilization of AR protein [23]. Androgen-induced ARLNC1 stabilizes AR mRNA through RNA-RNA hybridization, enhancing post-transcriptional AR expression levels [24]. Thus, LncRNAs, particularly AR-regulated LncRNAs, constitute an important regulatory layer in AR reactivation. In this study, we found a significant positive correlation

between FLJ and AR expression in the same batch of PCa tissues. Furthermore, we discovered that AR can regulate FLJ transcription in CRPC cells through a traditional transcription factor activation mechanism. These findings suggest that FLJ is a novel molecule activated by AR and may explain the high expression of FLJ in CRPC cells, which could be related to AR reactivation.

The function of LncRNAs is often associated with their unique subcellular localization [25]. We found that FLJ is primarily localized in the cytoplasm of CRPC cells, where it exerts dual regulatory functions on AR. On the one hand, FLJ inhibits AR nuclear translocation, suppressing the conventional androgen-dependent growth regulation pathway. On the other hand, FLJ prevents the degradation of AR protein retained in the cytoplasm, mediating micro-androgen-induced autophagy activation, thereby enabling CRPC cells to survive in a castration environment and develop drug resistance. This discovery reveals a novel mechanism by which CRPC cells survive and develop resistance under micro-androgen influence, offering new insights into the mechanisms maintaining high AR levels in CRPC.

Both autophagy and LncRNAs have the potential to promote or inhibit cancer progression. Persistent autophagy is considered a key mechanism underlying cancer treatment resistance and immune evasion, and safely reducing autophagy flux is a promising strategy for the treatment of advanced cancer [26]. As research on LncRNAs has deepened in recent years, they have been shown to play significant roles in regulating autophagy in PCa. For example, LncRNA HULC inhibits autophagy by modulating Beclin-1 levels and targeting the mTOR pathway [27], while LncRNA SNHG1 inhibits autophagy by binding to EZH2 and regulating the PI3K-AKT-mTOR and Wnt- β -catenin pathways [28]. These studies establish LncRNAs as potential therapeutic targets for regulating cancer autophagy. However, most studies on LncRNA regulation of autophagy have focused on the classical mTOR pathway and its upstream regulatory molecules. Research has found that castration does not completely

(See figure on next page.)

Fig. 6 LncFLJ prevents AR from entering the nucleus and stabilizes its protein in the cytoplasm. **A** The expression of AR and target proteins following FLJ knockdown was assessed by WB. **B** The expression of AR and target genes following FLJ knockdown was evaluated by qRT-PCR. **C** The lncLocator website was used to predict the subcellular localization of FLJ. **D** The subcellular localization of FLJ in 22Rv1 cells was assessed by RNA-FISH, with a scale bar of 50 μ m. **E** The subcellular localization of FLJ in 22Rv1 cells after RNA nuclear and cytoplasmic separation was evaluated by qRT-PCR. **F, G** The subcellular distribution of AR after FLJ knockdown was assessed by immunofluorescence, with a scale bar of 25 μ m. **H** The subcellular distribution of AR and target proteins after nuclear and cytoplasmic separation was assessed by WB. **I** The regulation of cytoplasmic AR protein degradation rate following FLJ knockdown was evaluated by WB

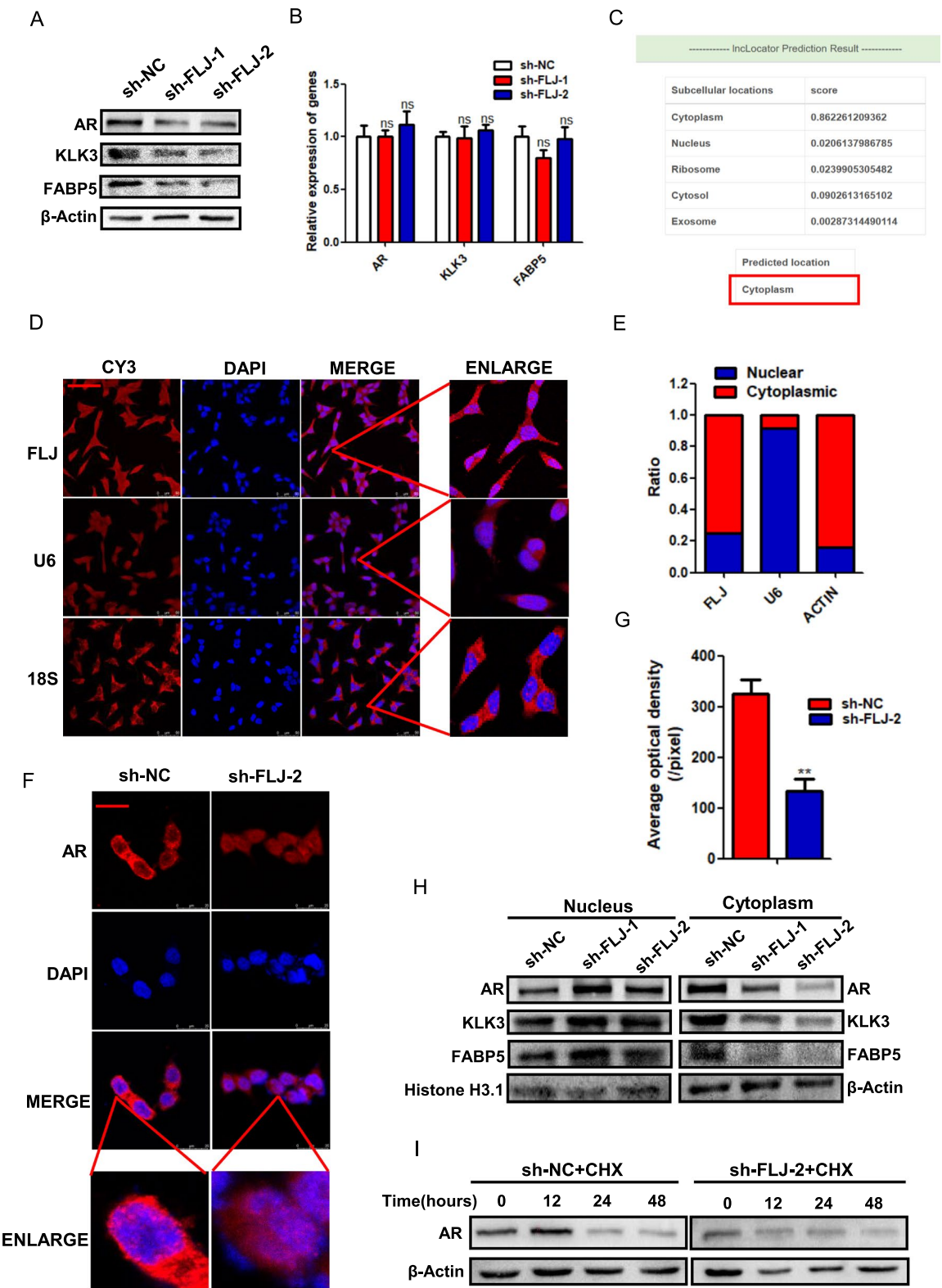


Fig. 6 (See legend on previous page.)

eliminate androgens in the prostate tumor microenvironment, and these residual androgens are involved in nearly all AR-mediated signaling mechanisms in CRPC [17]. In this study, we revealed a novel pathway of lncRNA-regulated autophagy—specifically, androgen-induced autophagy. FLJ regulates CRPC cell proliferation and castration sensitivity through AR-mediated androgen-induced autophagy. The AR-mediated autophagy pathway in PCa has been confirmed [17, 18], and we are the first to study the regulatory pattern of lncRNAs in this pathway, identifying the impact of lncRNAs on the biological functions and drug sensitivity of CRPC cells.

Overcoming CRPC and its resistance to enzalutamide (ENZA) has been a major challenge in PCa treatment and remains the leading cause of death in prostate cancer patients. Compared with protein-coding genes and miRNAs, lncRNAs are gradually emerging as new targets in cancer treatment [29]. For example, antisense oligonucleotides targeting MALAT1 have successfully prevented lung cancer metastasis in vivo [30]. The overexpression of GAS5 inhibits glioma growth by targeting miR-222 and prolongs survival [31]. In this study, we demonstrated that FLJ inhibits CRPC cell proliferation and enhances the biological functions related to simulated castration and ENZA drug sensitivity. More importantly, knocking down FLJ significantly inhibited tumor growth and enhanced the efficacy of ENZA treatment. These results suggest that FLJ is a novel and promising therapeutic target for CRPC treatment.

Currently, cancer treatments predominantly focus on proteins, while the rapidly evolving field of lncRNA-based therapies is garnering increasing attention. In this study, we identified the pivotal role of the novel lncRNA FLJ in the development of resistance to castration-resistant prostate cancer (CRPC). Targeting FLJ represents a promising and innovative therapeutic approach for CRPC. Several strategies exist for targeting long non-coding RNAs (lncRNAs). One such strategy involves “Gapmer” antisense oligonucleotides (ASOs), which bind to their complementary target lncRNAs, inducing their degradation by RNaseH1 in the nucleus. Another approach employs steric blocker ASOs (SB-ASOs), which disrupt

the interactions between lncRNAs and other molecular partners, thereby inhibiting their activity throughout the cell [32, 33]. Furthermore, small interfering RNAs (siRNAs), which consist of double-stranded RNA, have emerged as potential therapeutic agents for targeting lncRNAs. Advances in siRNA chemistry and formulation have significantly enhanced their therapeutic efficacy, allowing for prolonged in vivo activity. These innovations now make it possible to administer siRNA treatments on a 6-month dosing cycle, representing a major improvement over the daily or weekly administration required for traditional small molecule drugs [34]. Several oncogenic lncRNAs, including HOTAIR, MALAT1, CCAT1, lncRNA-ATB, and CRNDE, have been effectively targeted using siRNAs [35]. Another strategy for modulating lncRNAs involves the use of classical small molecules. For example, compound X1 has been shown to bind to and destabilize the lncRNA XIST, suppressing the growth and metastasis of breast cancer cells both in vitro and in vivo [36]. With the ongoing advancements in sequencing technologies and biotechnological innovations, lncRNA-targeted therapies are emerging as one of the most promising and transformative areas of cancer treatment in the near future.

In summary, our study reveals a novel AR-interacting lncRNA-FLJ that promotes CRPC cell proliferation while suppressing sensitivity to simulated castration and antiandrogen drugs through AR-mediated micro-androgen-induced autophagy. Targeting FLJ may represent a new potential therapeutic approach for CRPC patients.

Conclusions

Herein, the elevated androgen receptor (AR) environment in castration-resistant prostate cancer (CRPC) induces the expression of the novel long non-coding RNA (lncRNA) FLJ. FLJ inhibits AR nuclear translocation, thereby disrupting the conventional androgen-dependent cell survival pathway while concurrently preventing AR protein degradation in the cytoplasm. Additionally, FLJ induces autophagy through AR-mediated low-dose androgen stimulation, promoting CRPC cell proliferation and inhibiting sensitivity to castration-mimetic conditions and anti-androgen therapies in vitro (Fig. 8).

(See figure on next page.)

Fig. 7 Critical Role of FLJ in Regulating ENZA Treatment Sensitivity and Tumor Development. **A** Schematic of the in vivo experimental procedure. **B** Graph showing changes in subcutaneous tumor volume. **C** Weight change graph for nude mice. **D** Diagram of excised tumors. **E** Chart displaying the weights of excised tumors. **F** HE staining and IHC analysis of AR, LC3B, and Ki67 in tumor tissue sections, with a scale bar of 50 μ m. **G** Quantification of AR IHC scores in tumor tissue sections. **H** Quantification of LC3B IHC scores in tumor tissue sections. **I** Quantification of Ki67 IHC scores in tumor tissue sections. **J** qRT-PCR analysis of FLJ expression in RNA extracted from tumor tissues

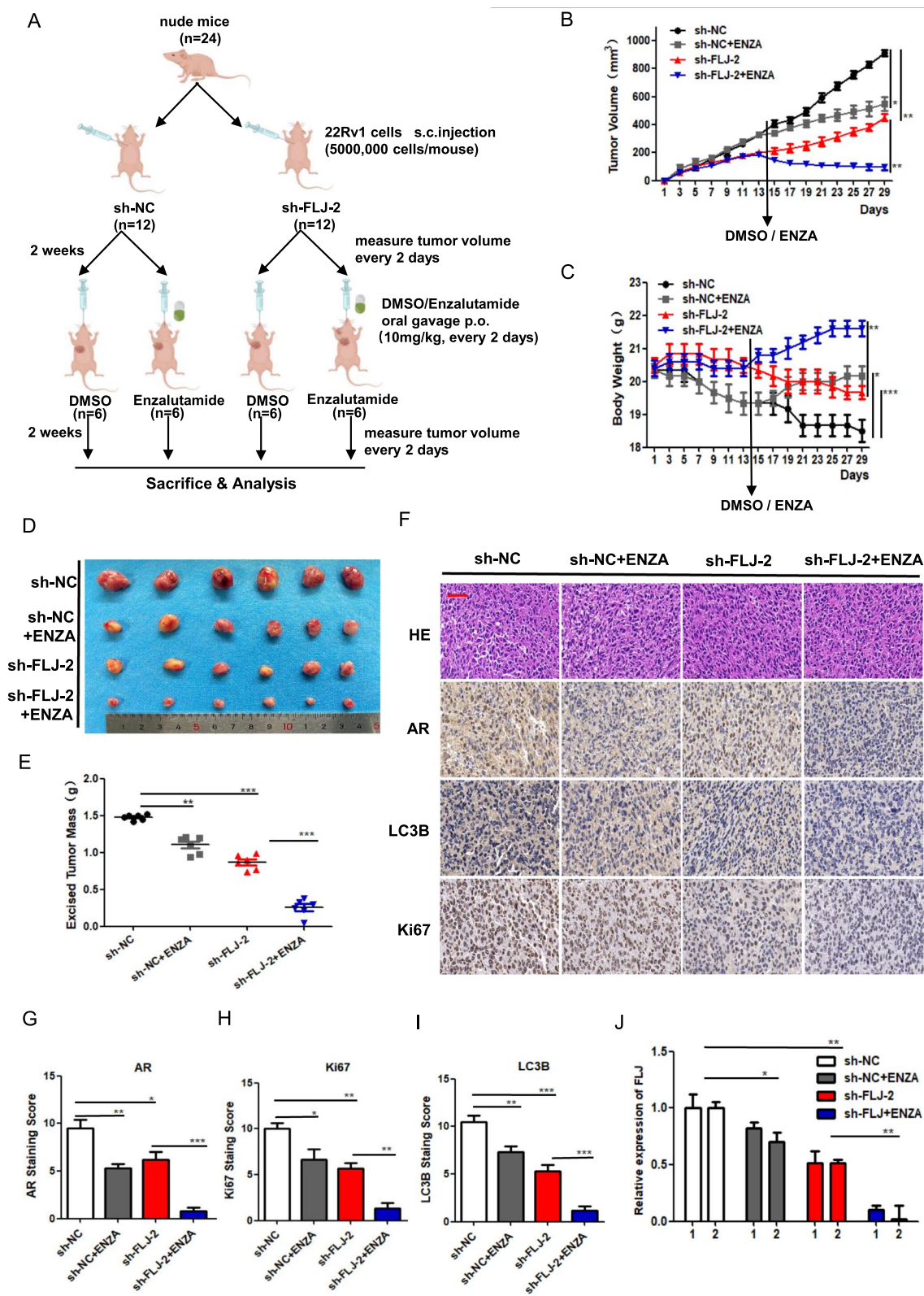


Fig. 7 (See legend on previous page.)

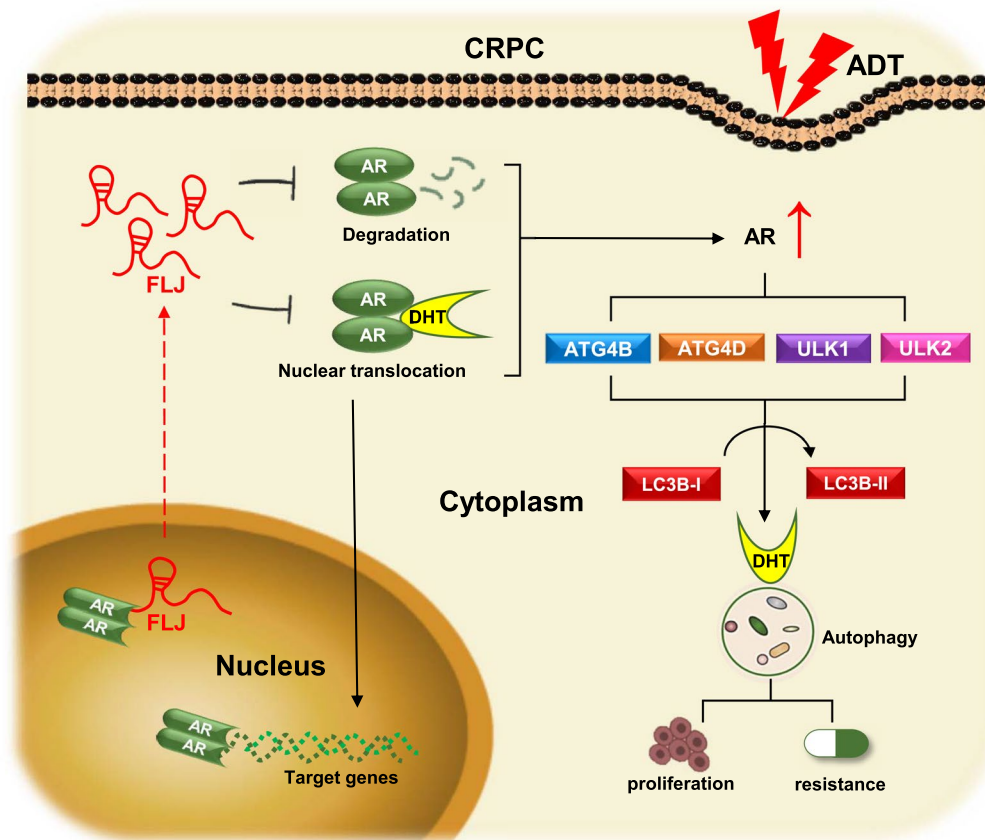


Fig. 8 Schematic diagram displays the function of FLJ in CRPC. Elevated androgen receptor (AR) levels in castration-resistant prostate cancer (CRPC) stimulate the expression of a novel long non-coding RNA FLJ. FLJ inhibits AR translocation to the nucleus, disrupting the conventional androgen-dependent survival pathway. Concurrently, FLJ stabilizes AR protein in the cytoplasm by preventing its degradation. Additionally, FLJ induces autophagy through AR-mediated low-dose androgen stimulation, promoting CRPC cell proliferation and re-sensitizing these cells to castration-mimetic conditions and anti-androgen therapies in vitro

Supplementary Information

The online version contains supplementary material available at <https://doi.org/10.1186/s12967-025-06294-9>.

Supplementary Material 1. Figure S1 **A**. FLJ expression levels in androgen deprivation therapy (ADT) responding or castrate-resistant patients. **B-C**. Analysis of FLJ expression in human prostate cancer, stratified by tumor stage (B) and Gleason scores (C), was conducted using data obtained from the TCGA database. **D**. Pearson correlation analysis of FLJ and AR expression based on data from TCGA database. Figure S2 **A-B**. The influence of FLJ knockdown on cell cycle distribution was analyzed by flow cytometry. **C-D**. The impact of FLJ knockdown on cell apoptosis was evaluated using flow cytometry. **E**. Apoptosis-related markers following FLJ knockdown were detected through Western blot analysis. **F**. Autophagy-related markers following FLJ knockdown were identified via Western blot analysis. **G**. Key proteins in the PI3K/AKT/mTOR signaling pathway after FLJ knockdown were detected by Western blot analysis. **H**. The subcellular localization of FLJ in C4-2 and C4-2B cells after RNA nuclear and cytoplasmic separation was evaluated by qRT-PCR.

Acknowledgements

We appreciate the samples provided by the First Affiliated Hospital of Chongqing Medical University. We appreciate the technical support provided by SHBIO (Shanghai, China). Additionally, Dr. Cheng wishes to thank companionship from Dr. Wu. You are the key word in my life, will you marry me?

Author contributions

XHW, CLL, TMC and LPO designed this study; YYW, SJC, YLQ, LLW, TL, and YBZ performed the experiments; YYW, SJC, and YLQ analyzed the data; YYW and YBZ organized the figures and drafted the initial manuscript; SJC and LPO revised this manuscript; all authors read and approved the final manuscript.

Funding

This work was supported in part by the Chongqing Overseas Chinese Returned Entrepreneurship and Innovation Support Program of P. R. China (Grant No. cx2021095); Chongqing Natural Science Foundation (no. CSTB2022NSCQ-BHX0686); Chongqing Natural Science Foundation (no. CSTB2024NSCQ-MSX0141).

Availability of data and materials

The supporting data and materials are provided in Additional Figures and Tables.

Declarations

Ethics approval and consent to participate

All experiments were approved by the Ethics Committee of Chongqing Medical University. Approval Number: 2022- K275.

Consent for publication

All authors read and approved the final manuscript.

Competing interests

The authors declare that they have no competing interests.

Author details

¹Department of Clinical Laboratory, Chongqing University Fuling Hospital, Chongqing, China. ²Key Laboratory of Laboratory Medical Diagnostics, Chinese Ministry of Education, Chongqing Medical University, No.1, Yi-Xue-Yuan Road, Yu-Zhong District, Chongqing 400016, China. ³Basic Medicine Research and Innovation Center for Novel Target and Therapeutic Intervention, Ministry of Education, College of Pharmacy, Chongqing Medical University, Chongqing, China. ⁴Department of Urology, The First Affiliated Hospital of Chongqing Medical University, Chongqing, China.

Received: 5 November 2024 Accepted: 23 February 2025

Published online: 03 March 2025

References

- Bray F, Laversanne M, Sung H, Ferlay J, Siegel RL, Soerjomataram I, Jemal A. Global cancer statistics 2022: GLOBOCAN estimates of incidence and mortality worldwide for 36 cancers in 185 countries. *CA Cancer J Clin*. 2024;74(3):229–63.
- Siegel RL, Miller KD, Wagle NS, Jemal A. Cancer statistics, 2023. *CA Cancer J Clin*. 2023;73(1):17–48.
- Basak D, Gregori L, Johora F, Deb S. Preclinical and clinical research models of prostate cancer: a brief overview. *Life (Basel)*. 2022;12(10):1607.
- Corti M, Lorenzetti S, Ubaldi A, Zilli R, Marcocchia D. Endocrine disruptors and prostate cancer. *Int J Mol Sci*. 2022;23(3):1216.
- Mostaghel EA. Beyond T and DHT—novel steroid derivatives capable of wild type androgen receptor activation. *Int J Biol Sci*. 2014;10(6):602–13.
- Gogola S, Rejzner M, Bahmad HF, Alloush F, Omarzai Y, Poppiti R. Anti-cancer stem-cell-targeted therapies in prostate cancer. *Cancers (Basel)*. 2023;15(5):1621.
- Kong P, Zhang L, Zhang Z, Feng K, Sang Y, Duan X, Liu C, Sun T, Tao Z, Liu W. Emerging proteins in CRPC: functional roles and clinical implications. *Front Oncol*. 2022;12: 873876.
- Chen X, Lu J, Xia L, Li G. Drug resistance of enzalutamide in CRPC. *Curr Drug Targets*. 2018;19(6):613–20.
- Chandrasekar T, Yang JC, Gao AC, Evans CP. Mechanisms of resistance in castration-resistant prostate cancer (CRPC). *Transl Androl Urol*. 2015;4(3):365–80.
- McCabe EM, Rasmussen TP. lncRNA involvement in cancer stem cell function and epithelial-mesenchymal transitions. *Semin Cancer Biol*. 2021;75:38–48.
- Taheri M, Khoshbakht T, Jamali E, Kallenbach J, Ghafouri-Fard S, Banihmad A. Interaction between non-coding RNAs and androgen receptor with an especial focus on prostate cancer. *Cells*. 2021;10(11):3198.
- Zhang Y, Pitchiaya S, Cieřlik M, Niknafs YS, Tien JC, Hosono Y, Iyer MK, Yazdani S, Subramaniam S, Shukla SK, et al. Analysis of the androgen receptor-regulated lncRNA landscape identifies a role for ARLNC1 in prostate cancer progression. *Nat Genet*. 2018;50(6):814–24.
- Kim KH, Lee MS. Autophagy—a key player in cellular and body metabolism. *Nat Rev Endocrinol*. 2014;10(6):322–37.
- Amaravadi RK, Kimmelman AC, Debnath J. Targeting autophagy in cancer: recent advances and future directions. *Cancer Discov*. 2019;9(9):1167–81.
- Mele L, Del Vecchio V, Liccardo D, Prisco C, Schwerdtfeger M, Robinson N, Desiderio V, Tirino V, Papaccio G, La Noce M. The role of autophagy in resistance to targeted therapies. *Cancer Treat Rev*. 2020;88: 102043.
- Maiuri MC, Zalckvar E, Kimchi A, Kroemer G. Self-eating and self-killing: crosstalk between autophagy and apoptosis. *Nat Rev Mol Cell Biol*. 2007;8(9):741–52.
- Ding M, Jiang CY, Zhang Y, Zhao J, Han BM, Xia SJ. SIRT7 depletion inhibits cell proliferation and androgen-induced autophagy by suppressing the AR signaling in prostate cancer. *J Exp Clin Cancer Res*. 2020;39(1):28.
- Wen S, Niu Y, Lee SO, Chang C. Androgen receptor (AR) positive vs negative roles in prostate cancer cell deaths including apoptosis, anoikis, entosis, necrosis and autophagic cell death. *Cancer Treat Rev*. 2014;40(1):31–40.
- Zhang A, Zhao JC, Kim J, Fong KW, Yang YA, Chakravarti D, Mo YY, Yu J. lncRNA HOTAIR enhances the androgen-receptor-mediated transcriptional program and drives castration-resistant prostate cancer. *Cell Rep*. 2015;13(1):209–21.
- Huang S, Liao Q, Li W, Deng G, Jia M, Fang Q, Ji H, Meng M. The lncRNA PTTG3P promotes the progression of CRPC via upregulating PTTG1. *Bull Cancer*. 2021;108(4):359–68.
- Gu P, Chen X, Xie R, Han J, Xie W, Wang B, Dong W, Chen C, Yang M, Jiang J, et al. lncRNA HOXD-AS1 regulates proliferation and chemo-resistance of castration-resistant prostate cancer via recruiting WDR5. *Mol Ther*. 2017;25(8):1959–73.
- Schmitz SU, Grote P, Herrmann BG. Mechanisms of long noncoding RNA function in development and disease. *Cell Mol Life Sci*. 2016;73(13):2491–509.
- Malik R, Patel L, Prensner JR, Shi Y, Iyer MK, Subramaniam S, Carley A, Niknafs YS, Sahu A, Han S, et al. The lncRNA PCAT29 inhibits oncogenic phenotypes in prostate cancer. *Mol Cancer Res*. 2014;12(8):1081–7.
- Shukla S, Zhang X, Niknafs YS, Xiao L, Mehra R, Cieřlik M, Ross A, Schaeffer E, Malik B, Guo S, et al. Identification and validation of PCAT14 as prognostic biomarker in prostate cancer. *Neoplasia*. 2016;18(8):489–99.
- Statello L, Guo CJ, Chen LL, Huarte M. Gene regulation by long non-coding RNAs and its biological functions. *Nat Rev Mol Cell Biol*. 2021;22(2):96–118.
- Kumar A, Girisa S, Alqahtani MS, Abbas M, Hegde M, Sethi G, Kunnumakkara AB. Targeting autophagy using long non-coding RNAs (lncRNAs): new landscapes in the arena of cancer therapeutics. *Cells*. 2023;12(5):810.
- Chen C, Wang K, Wang Q, Wang X. lncRNA HULC mediates radioresistance via autophagy in prostate cancer cells. *Braz J Med Biol Res*. 2018;51(6): e7080.
- Chen J, Wang F, Xu H, Xu L, Chen D, Wang J, Huang S, Wen Y, Fang L. Long non-coding RNA SNHG1 regulates the Wnt/ β -catenin and PI3K/AKT/mTOR signaling pathways via EZH2 to affect the proliferation, apoptosis, and autophagy of prostate cancer cell. *Front Oncol*. 2020;10: 552907.
- Gutschner T, Diederichs S. The hallmarks of cancer: a long non-coding RNA point of view. *RNA Biol*. 2012;9(6):703–19.
- Gutschner T, Hämmerle M, Eissmann M, Hsu J, Kim Y, Hung G, Revenko A, Arun G, Stentrup M, Gross M, et al. The noncoding RNA MALAT1 is a critical regulator of the metastasis phenotype of lung cancer cells. *Cancer Res*. 2013;73(3):1180–9.
- Zhao X, Wang P, Liu J, Zheng J, Liu Y, Chen J, Xue Y. Gas5 exerts tumor-suppressive functions in human glioma cells by targeting miR-222. *Mol Ther*. 2015;23(12):1899–911.
- Rinaldi C, Wood MJA. Antisense oligonucleotides: the next frontier for treatment of neurological disorders. *Nat Rev Neurol*. 2018;14(1):9–21.
- Schmidt K, Weidmann CA, Hilimire TA, Yee E, Hatfield BM, Schneckloth JS Jr, Weeks KM, Novina CD. Targeting the oncogenic long non-coding RNA SLNCR1 by blocking its sequence-specific binding to the androgen receptor. *Cell Rep*. 2020;30(2):541–554.e545.
- Ray KK, Troquay RPT, Visseren FLJ, Leiter LA, Scott Wright R, Vikarunnessa S, Tallozy Z, Zang X, Maheux P, Lesogor A, et al. Long-term efficacy and safety of inclisiran in patients with high cardiovascular risk and elevated LDL cholesterol (ORION-3): results from the 4-year open-label extension of the ORION-1 trial. *Lancet Diabetes Endocrinol*. 2023;11(2):109–19.
- Coan M, Haefliger S, Ounzain S, Johnson R. Targeting and engineering long non-coding RNAs for cancer therapy. *Nat Rev Genet*. 2024;25(8):578–95.
- Aguilar R, Spencer KB, Kesner B, Rizvi NF, Badmalia MD, Mrozowicz T, Mortison JD, Rivera C, Smith GF, Burchard J, et al. Targeting Xist with compounds that disrupt RNA structure and X inactivation. *Nature*. 2022;604(7904):160–6.

Publisher's Note

Springer Nature remains neutral with regard to jurisdictional claims in published maps and institutional affiliations.